

Supplemental Document:

Electronic Structure Governed by On-center or Off-center indium:

LnOInS₂ (Ln=La, Ce, and Pr)

Hiroaki Ito^{a)}, Akira Miura^{*b)}, Yosuke Goto^{c)}, Yoshikazu Mizuguchi^{c)}, Chikako Moriyoshi^{d)}, Yoshihiro Kuroiwa^{d)}, Masaki Azuma^{e)}, Liu Jinjia^{f)}, Xiao-Dong Wen^{f)}, Shunta Nishioka^{g,h)}, Kazuhiko Maeda^{g)}, Yuji Masubuchi,^{b)} Nataly Carolina Rosero-Navarro^{a)}, Kiyoharu Tadanaga^{a)}

a) Graduate School of Chemical Sciences and Engineering, Hokkaido University, Kita 13, Nishi 8 Sapporo 060-8628, Japan, b) Faculty of Engineering, Hokkaido University, Kita 13, Nishi 8 Sapporo 060-8628, Japan
c) Department of Physics, Tokyo Metropolitan University, 1-1 Minami-osawa, Hachioji, Tokyo 192-0397, Japan, d) Department of Physical Science, Hiroshima University, 1-3-1 Kagamiyama, Higashihiroshima, Hiroshima 739-8526, Japan, e) Materials and Structures Laboratory, Tokyo Institute of Technology, Yokohama 226-8503, Japan f) State Key Laboratory of Coal Conversion, Institute of Coal Chemistry, Chinese Academy of Sciences, Taiyuan 030001, P. R. China, g) Department of Chemistry, School of Science, Tokyo Institute of Technology, 2-12-1-NE-2 Ookayama, Meguro-ku, Tokyo 152-8550, Japan, h) Japan Society for the Promotion of Science, Kojimachi Business Center Building, 5-3-1 Kojimachi, Chiyoda-ku, Tokyo 102-0083, Japan

Structural refinement results

Figure S1 and Table S1, S2, and S3 indicate the Rietveld refinement results for LaOInS₂ and PrOInS₂ with split In site models. Table S2, S3, and S4 show lattice parameters, atomic positions, and atomic displacement parameters for split In site models, respectively. The summary of crystallographic data of LaOInS₂ and PrOInS₂ refined with a fourth-order (anharmonic) displacement parameter, D_{2222} , for indium, and CeOInS₂ refined with second-order (harmonic) displacement parameters, U_{11} , U_{22} , U_{33} for indium are also summarized in Table S4, S5, and S6. The position of oxygen atoms were fixed for all refinements. Since the difference between lattice parameters of a and b were small, the refined lattice parameters were converged either $a > b$ or $b < a$, depending on the X-ray diffraction patterns. In order to compare the results, all the data were summarized as $b > a$ with D_{2222} although some refinements were converged with $a > b$ and D_{1111} .

Figure S1 depicts the Rietveld refinement profiles of LaOInS_2 and PrOInS_2 . The Rietveld refinements of synchrotron XRD data of LaOInS_2 and PrOInS_2 at 300 K were refined with split site models, and converged with comparable fitting parameters with that for anharmonic displacement models.

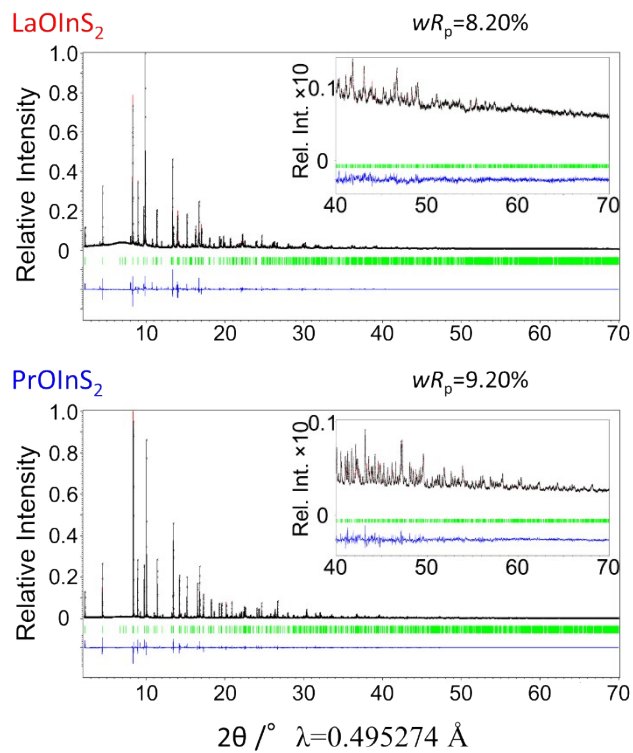


Figure S1 Rietveld refinement profile of LaOInS_2 and PrOInS_2 refined with split site models. Inset is expanded region of the XRD pattern.

Figure S2 shows the Rietveld refinement profiles of LaOInS_2 , CeOInS_2 , and PrOInS_2 at 300 K. Insets are expanded region of the XRD patterns. The Rietveld refinements of synchrotron XRD data of LaOInS_2 and PrOInS_2 with fourth-order (anharmonic) displacement parameter of indium result in good fitting. In CeOInS_2 , the refinement with fourth-order displacement parameter of indium showed the negative probability density. Thus, the structures of CeOInS_2 were refined with second-order displacement parameters.

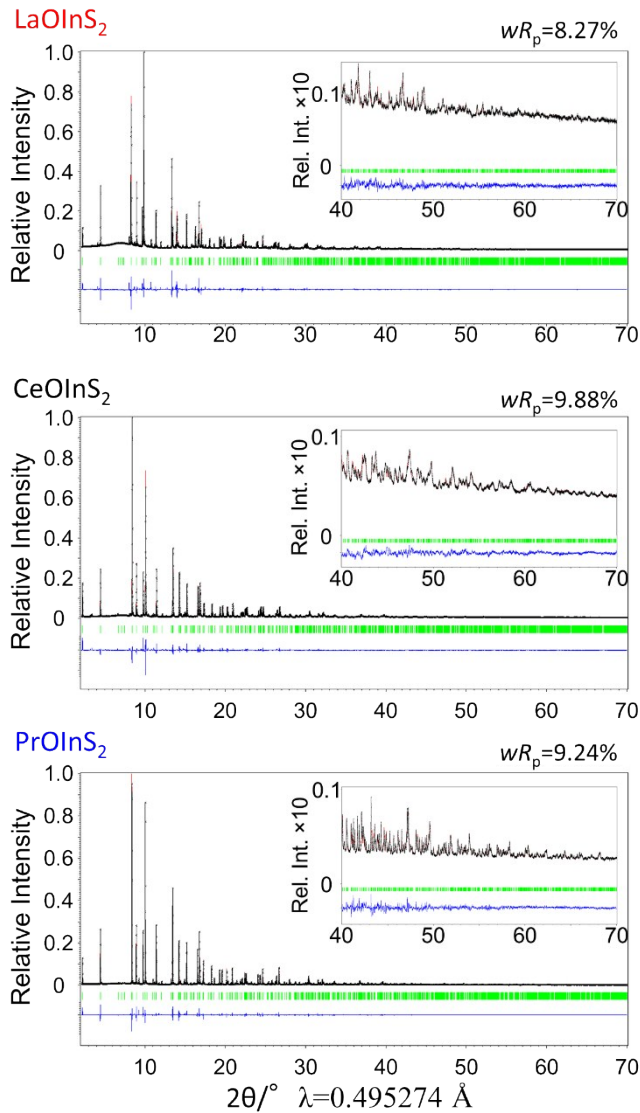


Figure S2 Rietveld refinement profile of LnOInS_2 at 300 K using anharmonic model. Inset is expanded region of the XRD pattern.

Table S1 Lattice parameters of LaOInS₂ and PrOInS₂ at 300 K with split model with two In sites with half occupancy.

Phase	Space group	Lattice parameter/Å			R_{wp} %
		a	B	c	
LaOInS ₂	$P2_1/m$	4.06374(3)	4.07921(3)	12.67649(7)	8.20
PrOInS ₂	$P2_1/m$	3.996659(14)	4.001856(16)	12.72152(4)	9.20

Table S2 Atomic positions of LaOInS₂ and PrOInS₂ at 300 K with split model with two In sites with half occupancy.

Phase	Ln			S1			S2			O			In		
	x	Y	z	x	y	z	x	y	z	x	y	z	x	y	z
LaOInS ₂	1/4	1/4	0.09810(8)	1/4	1/4	0.4115(3)	1/4	1/4	0.7908(3)	3/4	1/4	0	1/4	1/4±0.1081(5)	0.60785(13)
PrOInS ₂	1/4	1/4	0.09586(4)	1/4	1/4	0.4125(2)	1/4	1/4	0.79437(19)	3/4	1/4	0	1/4	1/4±0.0879(6)	0.60861(7)

Table S3 Atomic displacement parameters of LaOInS₂ and PrOInS₂ at 300 K with split model.

Phase	$U_{iso}(Ln)/\text{Å}^2$	$U_{iso}(S1)/\text{Å}^2$	$U_{iso}(S2)/\text{Å}^2$	$U_{iso}(O)/\text{Å}^2$	$U_{eq}(In)/\text{Å}^2$	$U_{11}(In)/\text{Å}^2$	$U_{22}(In)/\text{Å}^2$	$U_{33}(In)/\text{Å}^2$
LaOInS ₂	0.00403(16)	0.0128(10)	0.0042(8)	0.009(3)	0.0359(11)	0.0519(16)	0.050(2)	0.0058(10)
PrOInS ₂	0.00359(9)	0.0106(5)	0.0062(4)	0.0014(12)	0.0343(8)	0.0484(12)	0.050(2)	0.0045(6)

Table S4 Lattice parameters of LaOInS₂, CeOInS₂, and PrOInS₂ at 300 K. A fourth-order (anharmonic) atomic displacement parameter was adopted for LaOInS₂, CeOInS₂.

Phase	Space group	Lattice parameter/Å			R_{wp} %
		<i>A</i>	<i>B</i>	<i>C</i>	
LaOInS ₂	$P2_1/m$	4.06374(3)	4.07919(3)	12.67649(7)	8.27
CeOInS ₂	$P2_1/m$	3.98000(7)	3.98582(6)	12.69515(10)	9.88
PrOInS ₂	$P2_1/m$	3.996654(15)	4.001852(16)	12.72153(4)	9.24

Table S5 Atomic positions of LaOInS₂, CeOInS₂, and PrOInS₂ at 300 K. A fourth-order atomic displacement parameter was adopted for LaOInS₂ and PrOInS₂.

Phase	<i>Ln</i>			S1			S2			O			In		
	<i>x</i>	<i>y</i>	<i>z</i>	<i>x</i>	<i>y</i>	<i>z</i>	<i>x</i>	<i>y</i>	<i>Z</i>	<i>x</i>	<i>y</i>	<i>z</i>	<i>x</i>	<i>y</i>	<i>z</i>
LaOInS ₂	1/4	1/4	0.09806(8)	1/4	1/4	0.4116(3)	1/4	1/4	0.7909(3)	3/4	1/4	0	1/4	1/4	0.60783(13)
CeOInS ₂	1/4	1/4	0.09857(7)	1/4	1/4	0.4080(3)	1/4	1/4	0.7961(3)	3/4	1/4	0	1/4	1/4	0.60786(10)
PrOInS ₂	1/4	1/4	0.09587(5)	1/4	1/4	0.4125(2)	1/4	1/4	0.79440(19)	3/4	1/4	0	1/4	1/4	0.60860(7)

Table S6 Atomic displacement parameters of LaOInS₂, CeOInS₂, and PrOInS₂ at 300 K. A fourth-order atomic displacement parameter, D_{2222} , was adopted for LaOInS₂ and PrOInS₂. $U_{12} = U_{13} = U_{23} = 0$

Phase	$U_{iso}(Ln)/\text{Å}^2$	$U_{iso}(S1)/\text{Å}^2$	$U_{iso}(S2)/\text{Å}^2$	$U_{iso}(O)/\text{Å}^2$	$U_{eq}(In)/\text{Å}^2$	$U_{11}(In)/\text{Å}^2$	$U_{22}(In)/\text{Å}^2$	$U_{33}(In)/\text{Å}^2$	$D_{2222}(In)/\text{Å}^4$
LaOInS ₂	0.00386(16)	0.0113(10)	0.0034(8)	0.009(3)	0.0862(11)	0.0538(16)	0.198(3)	0.0072(10)	-5.87(11)
CeOInS ₂	0.00459(14)	0.0129(8)	0.0036(6)	0.0056	0.0449(10)	0.096(2)	0.0259(17)	0.0129(8)	0
PrOInS ₂	0.00333(9)	0.0108(5)	0.0062(5)	0.0018(12)	0.0637(8)	0.0497(12)	0.137(2)	0.0045(6)	-1.34(6)

Figure S3 and Figure S4 shows the probability density functions of indium in In-S₆ octahedra in CeOInS₂ and PrOInS₂, respectively. The diffraction data for PrOInS₂ at 450 K was refined with second-order displacement parameters, since the probability density function curve of indium determined using fourth-order displacement parameters has negative values. The probability densities along the *b* axis for both CeOInS₂ and PrOInS₂ were high at the center of In-S₆ octahedron. The width of the probability density functions became narrower as the temperature increased.

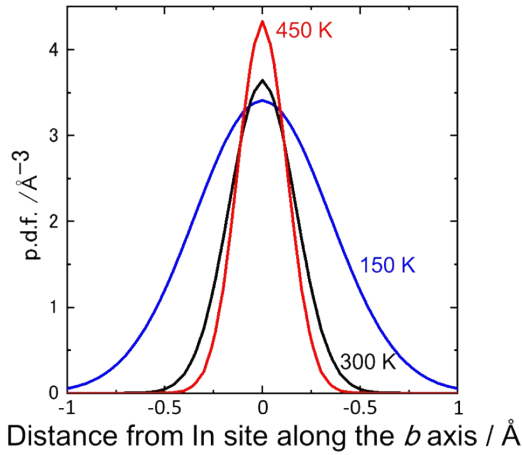


Figure S3 Probability density functions of indium in CeOInS₂ along the *b* axis.

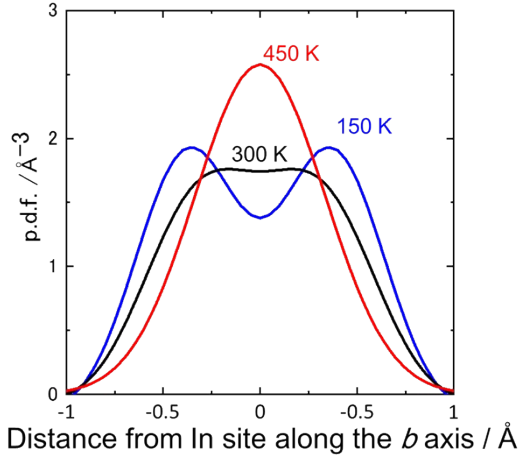


Figure S4 Probability density functions of indium in PrOInS₂ along the *b* axis.

The potential energy curves for indium in LaOInS₂, CeOInS₂, and PrOInS₂ at 300 K were calculated from respective probability density function. Figure S5 shows the potential curves along the *b* axis. At 300 K, the energy barrier at the center of In-S₆ octahedron was about 14 meV for LaOInS₂ and 0.21 meV for PrOInS₂. Since these values were smaller than kinetic energy, indium in In-S₆ octahedron was likely to move along the *b* axis.

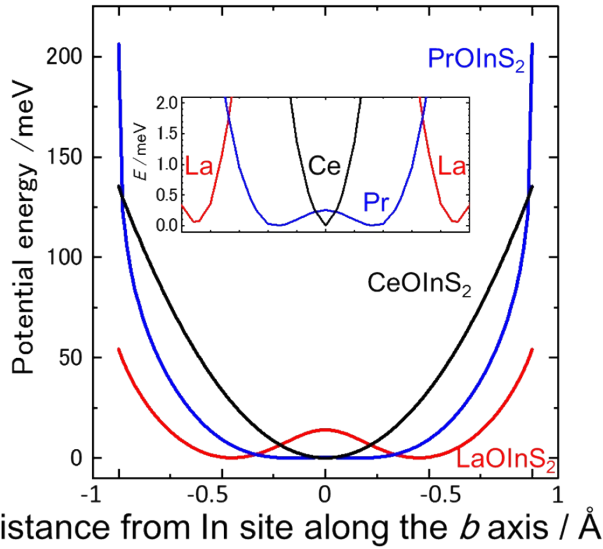


Figure S5 Potential curves for indium in LaOInS_2 , CeOInS_2 , and PrOInS_2 at 300 K. Inset is expanded region around the center of In-S_6 octahedron.

Fourier transforms f or In K-edge XAFS spectra

Figure S6 indicates normalized Fourier transforms of In K-edge XAFS spectra for LaOInS_2 and NaInS_2 . Although both compounds have the structure involving In-S_6 octahedra, the octahedra in LaOInS_2 are distorted and In in LaOInS_2 exhibits high atomic displacement parameters than those of NaInS_2 . The prominent peak was at 2.11 Å for NaInS_2 and 2.05 Å for LaOInS_2 . Wide and small peaks can be explained distorted octahedral of LaOInS_2 as well as their large atomic displacements.

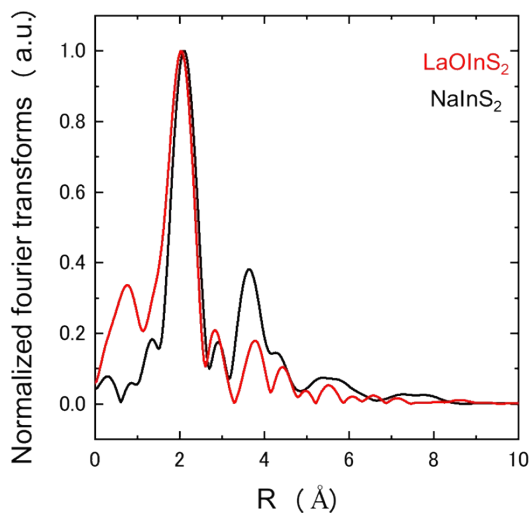


Figure S6 Radial distribution function for In of LaOInS_2 and NaInS_2 .

Computational results

For preliminary calculation, the PBE-GGA method was used for the optimization of the crystal structure models and calculation of electronic structures. The simulation models and calculation data is shown in Figure S7 and Table S7. The relative lattice energy per unit cells and bandgaps were slightly different of each models, and models with large displacement of indium were more stable than other models. Model 0 to Model 2 were the models of displacement in one unit cell and involve two indium atoms. The effect of superlattice structures was examined by using Model 3 and Model 4, which contained two unit cells and where four indium atoms were ordered. The round marks represents indium atoms at the center of In-S₆ octahedron and the arrows indicate the direction of displacement of indium along the *b* axis. Table S7 shows the summary of models calculated by GGA-PBE method. In table S7, $\Delta E/eV$, Δb_{av} , and E_g are the energy differences, average displacements of In along the *b* axis, and bandgaps calculated from GGA-PBE function, respectively. Table S5 shows that structures with large displacement of indium were more stable and possessed wider bandgaps than that of Model 0. Although GGA-PBE approach underestimate band gaps due to unphysical self-Coulomb repulsion^[1-3], the energy of bandgap changed with the displacement of In.

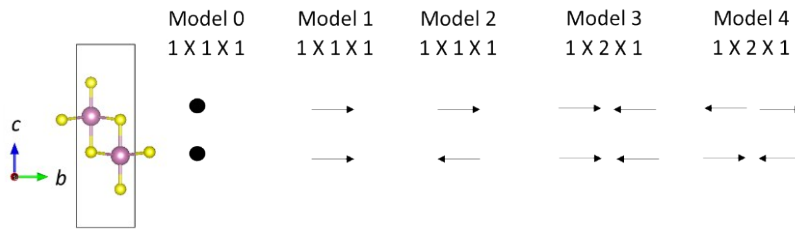


Figure S7 Structural models used for the DFT calculation based on GGA-PBE approach

Table S7 Summary of optimized structures based on GGA-PBE approach.

Model	$\Delta E/eV(\text{unitcell})$	$\Delta b_{av} / \text{nm}$	E_g / eV
0	0.000	0.000	0.88
1	-0.092	0.055	1.27
2	-0.089	0.043	1.01
3	-0.015	0.057	0.85
4	-0.016	0.044	0.87

References

- 1 Perdew, J. P.; Levy, M. *Phys. Rev. Lett.* 1983, **51**, 1884– 1887.
- 2 Sham, L. J.; Schlüter, M. *Phys. Rev. Lett.* 1983, **51**, 1888– 1891.
- 3 Mori-Sánchez, P.; Cohen, A. J.; Yang, W. *Phys. Rev. Lett.* 2008, **100**, 146401.